We can, of course, in principle extend this model without difficulty to include rate coefficients dependent on the polymer to any finite size. However, if this dependence had to be carried to any appreciable length of polymer, calculations in this style would become very onerous indeed. In such circumstances it might be preferable to reformulate the whole problem in terms of a continuous dependence of the rate coefficients on size, and to seek approximate solutions to the resulting differential equations in terms of suitable distributional forms.

Manuscript received March 28, 1966; revision received August 1, 1966; paper accepted August 1, 1966. Paper presented at A.I.Ch.E. Philadelphia meeting.

Momentum Transfer in Climbing Film Flow in Annular Duct

D. H. KIM and J. G. KNUDSEN

Oregon State University, Corvallis, Oregon

The characteristics of upward gas–liquid flow in a vertical annular duct were investigated. The flow regime studied was the climbing film regime in which water flowed as a film up the inner core of the annulus while air flowed in the annular space, the outer wall of the annulus remaining dry. Friction losses, air velocity distributions, and film characteristics were studied, the latter by photographing the climbing film through the transparent outer tube. Friction loss and film thickness were correlated with Lockhart–Martinelli parameters, X, Φ, and R_L. The presence of the climbing film caused the point of maximum velocity of the air profile to move toward the outer tube, indicating that the film created a rough wall condition. The inner portion of the velocity profile was correlated by Nikuradse's rough tube equation, while the outer portion was correlated by a logarithmic equation which previous workers have reported for single-phase flow. Kapitza's theory of wave formation was applied to the climbing film and was found to predict reasonable values for the mean film thickness. However, it failed to predict reliable values for the wavelength of surface waves.

In vertically upward gas-liquid flow in closed ducts, several regimes of flow occur which are a function of the gas and liquid flow rates. These regimes can be observed sequentially as the gas flow rate increases at constant liquid flow rate. At low gas flow rates, the gas flows upward as small bubbles. With increasing gas flow rates, the gas assumes the form of large slugs and ultimately forms a continuous core while the liquid flows as a film up the walls of the duct. This latter regime of flow is the annular flow or climbing film regime. Similar regimes are also observed in a single heated tube in which boiling occurs.

The climbing film regime of two-phase flow has been the subject of many investigations. These studies have been stimulated mainly by the variety of process equipment such as water tube boilers, wetted-wall columns, and coolant channels of nuclear reactors in which such flow occurs. High heat and mass transfer rates occur in climbing film flow. An understanding of the basic transport phenomena taking place in climbing film flow will provide a sounder basis for design of process equipment.

Most previous investigators have used smooth pipes and narrow rectangular ducts to study the various characteristics of climbing film flow. While such ducts operate satisfactorily and provide reliable data, it is not possible to observe the liquid film directly, even though the duct wall is transparent.

In the present study, a long annular duct was employed in which air flowed in the annular space and a water film climbed up the concentric inner core. The outer dry tube was transparent so that the film could be observed directly. It was possible to determine values of momentum flux from velocity profile measurements.

An attempt has been made to investigate both the mechanics of the air flow in the annular duct as well as the mechanics of flow of the climbing film.

THEORETICAL BACKGROUND

Single-Phase Turbulent Flow in Annuli

Friction losses for single-phase flow in smooth annuli have usually been correlated with the hydraulic diameter used as the characteristic length in defining the friction factor and Reynolds number. The correlation is satisfactory for annuli in which $0.2 < \alpha < 0.8$. Prengle and Rothfus (*13*) defined a Reynolds number based upon the equivalent diameter of the outer portion of annular velocity profile.

$$N_{Re2} = \frac{4r_H U\rho}{\mu} \tag{1}$$

where

$$r_H = 2r_2(1 - \lambda^2)$$

By defining a friction factor

$$f_2 = \frac{2\tau_2 g_c}{\rho U^2} \tag{2}$$

the workers found that

$$1/\sqrt{f_2} = 4.0 \log (N_{Re2}\sqrt{f_2}) - 0.4 \tag{3}$$

Equation (3) is identical with the Nikuradse (*11*) friction factor–Reynolds number relation for smooth tubes.

Equations (1), (2), and (3) require a knowledge of the position of the point of maximum velocity r_m. For laminar flow, this radius is determined theoretically as (7)

$$\lambda^2 = \frac{1-\alpha^2}{\ln(1/\alpha^2)} \tag{4}$$

Several investigators (*6, 13*) have reported that Equation (4) also predicts the position of maximum velocity for turbulent flow. However, recent accurate measurements by Brighton and Jones (*1*) indicate that the position of maximum velocity for turbulent flow in smooth annuli is closer to the inner tube than for laminar flow. Macagno and McDougall (*10*) have theoretically derived the position of maximum velocity for turbulent flow in annuli and predict values somewhat closer to the inner tube than Brighton and Jones obtained experimentally.

For steady turbulent flow in annuli a momentum balance on an incremental length of flowing fluid shows (7)

$$\tau_1 = \left(\frac{-dP_f}{dx}\right)\left(\frac{r_2}{2}\right)\left(\frac{\lambda^2-\alpha^2}{\alpha}\right) \tag{5}$$

$$\tau_2 = \left(\frac{-dP_f}{dx}\right)\left(\frac{r_2}{2}\right)(1-\lambda^2) \tag{6}$$

$$\frac{\tau_1}{\tau_2} = \frac{\lambda^2-\alpha^2}{\alpha(1-\lambda^2)} \tag{7}$$

Climbing Film Flow in Annuli

This investigation of climbing film flow in an annular duct was concerned with the liquid film moving upward on the inner tube and the remaining annular space being filled with a turbulent air stream.

Figure 1*a* shows a section of the flow system investigated. Momentum balances over an incremental length on the combined stream, the liquid film, the air stream, the portion of the air stream inside the point of maximum velocity, and the portion outside the point of maximum velocity give the following equations for momentum transfer (5):

$$\tau_1 = \frac{1}{\alpha}\left[\alpha_i\tau_i - \left(\frac{dP}{dx} + \rho_L\frac{g}{g_c}\right)\left(\frac{r_2}{2}\right)(\alpha_i^2-\alpha^2)\right] \tag{8}$$

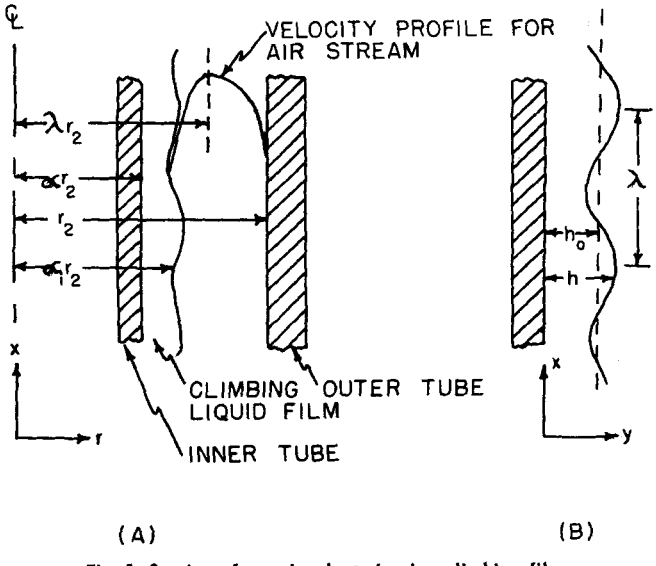

Fig. 1. Section of annular duct showing climbing film.

$$\tau_2 = -\left(\frac{dP}{dx} + \rho_g\frac{g}{g_c}\right)\left(\frac{r_2}{2}\right)(1-\lambda^2) \tag{9}$$

$$\tau_i = \tau_2\frac{\alpha_i(\lambda^2-\alpha_i^2)}{(1-\lambda^2)} \tag{10}$$

Equations (8), (9), and (10) are based upon the assumptions that there is no mass transfer between the gas and liquid either by diffusion or entrainment, and that kinetic energy terms are negligible. These relationships indicate that τ_1, τ_2, and τ_i may be determined if the pressure gradient, point of maximum velocity of the air stream, and thickness of the climbing film are known.

Application of Kapitza's Theory of Wave Formation to the Climbing Film

The upward flowing liquid film on the inner core of the annulus is considered to be of negligible thickness compared to the diameter of the inner core so that curvature may be neglected. Hence the motion of the liquid film is quasi two-dimensional, and by assuming laminar motion, the simplified momentum and continuity equations of flow are (see Figure 1*b*)

$$\frac{\partial u}{\partial t} + u\frac{\partial u}{\partial x} + v\frac{\partial u}{\partial y} = -\frac{1}{\rho}\frac{\partial P}{\partial x} + \nu\frac{\partial^2 u}{\partial y^2} - g \tag{11}$$

$$0 = \frac{\partial P}{\partial y} \tag{12}$$

$$\frac{\partial u}{\partial x} + \frac{\partial v}{\partial y} = 0 \tag{13}$$

Four boundary conditions beside zero initial condition are necessary to solve the equations

$$\text{at } y = 0 \quad u = v = 0 \tag{14}$$

$$\text{at } y = h(x,t) \quad \frac{\partial u}{\partial y} = \frac{\tau_i(x,t)}{\mu} \tag{15}$$

$$P = P_\sigma(x,t) + P_g(x) \tag{16}$$

The momentum transferred from the gas to the liquid is described by $\tau_i(x,t)$. The pressure of the liquid film at the interface must be equal to the summation of the air pressure P_g and the surface pressure P_σ, due to the surface tension. With small deformations of the surface in one direction, the surface pressure may be expressed as given by Laplace's equation on pressure discontinuity at the interface:

$$P_\sigma = -\sigma\frac{\partial^2 h}{\partial x^2} \tag{17}$$

where σ is the surface tension (*8*).

Since the pressure is not a function of y [Equation (12)], the pressure in Equation (11) can be replaced with the boundary condition

$$y = h(x,t), \quad P = P_\sigma + P_g \tag{16}$$

The continuity equation is rearranged to

$$v = -\int_o^y \frac{\partial u}{\partial x}dy = \frac{\partial h}{\partial t} \tag{18}$$

Hence, the final equations of flow for the climbing film are

$$\frac{\partial u}{\partial t} + u\frac{\partial u}{\partial x} - \left(\int_o^y \frac{\partial u}{\partial x}dy\right)\frac{\partial u}{\partial y} = -\frac{\sigma}{\rho}\frac{\partial^3 h}{\partial x^3} - \frac{1}{\rho}\frac{\partial P_g}{\partial x} + \nu\frac{\partial^2 u}{\partial y^2} - g \tag{19}$$

$$\frac{\partial h}{\partial t} = -\frac{\partial}{\partial x}\int_o^y u dy \qquad (20)$$

with boundary conditions as indicated by Equations (14) and (15).

Equations (19) and (20) are solved by determining first an approximate velocity profile by means of the following simplifying assumptions:

1. Convective terms are negligible
2. $\left(\frac{\partial u}{\partial y}\right)_{y=h} = \frac{\tau_i}{\mu}$ [constant] [that is, film thickness is assumed constant]
3. $P = P_g(x)$ [pressure due to surface tension is neglected]

Equation (19) becomes

$$\nu\frac{\partial^2 u}{\partial y^2} - g - \frac{1}{\rho_L}\frac{\partial P_g}{\partial x} = 0 \qquad (21)$$

which gives (5)

$$u = \frac{3}{h^2}\left(\frac{h}{2}\frac{\tau_i}{\mu} - \bar{u}\right)\left(\frac{y^2}{2} - hy\right) + \frac{\tau_i}{\mu}y \qquad (22)$$

when $\bar{u}$ is the average velocity in a film of thickness h, that is

$$\bar{u} = \frac{1}{h}\int_o^h u dy$$

Equation (22) is substituted into Equations (19) and (20), which are subsequently integrated with respect to y to obtain an expression for the mean film thickness and wavelength.

$$h_0 = \frac{\frac{3\tau_i}{2\rho} \pm \sqrt{\frac{9(\tau_i)^2}{4\rho^2} - 12\nu u_0\left(\frac{1}{\rho_L}\frac{\partial P_g}{\partial x} + g\right)}}{2\left(\frac{\partial P_g}{\partial x}\frac{1}{\rho} + g\right)} \qquad (23)$$

The wavelength $= \frac{2\pi}{k}$

$$= \frac{2\pi}{\sqrt{\left(\frac{\rho_L}{\sigma\pi r_1}\frac{Q}{h_0^2} - \frac{g_c\rho_L}{2\sigma\mu}\tau_i\right)\left(\frac{21}{20\pi r_1}\frac{Q}{h_0} - \frac{g_c}{\mu}\frac{3}{10}\tau_i h_0\right)}} \qquad (24)$$

The velocity profiles of the liquid film and the film thickness are, respectively

$$u = \frac{3}{h^2}\left[\frac{h}{2}\frac{\tau_i}{\mu} - u_0 - (c-u_0)\phi\cdots\right]\left[\frac{y^2}{2} - hy\right] + \frac{\tau_i}{\mu}y \qquad (25)$$

and

$$h = h_0(1+\phi) \qquad (26)$$

where

$$\phi = \sin k(x-ct) \qquad (27)$$

EXPERIMENTAL EQUIPMENT

The vertical annular duct consisted of a 3-in. I.D. Plexiglas outer tube and a concentric 1-in. O.D. aluminum inner tube. This inner tube was supported laterally by sets of centering screws located every 4 ft. The total length of the duct was about 35 ft. including a 20 ft. long test section. The first measurement location (bottom location) was 76 in. above the liquid injector and the second (top location) was 78 in. above the first. A flow diagram of the system is shown in Figure 2, while Figure 3 is a more detailed sketch of the test section

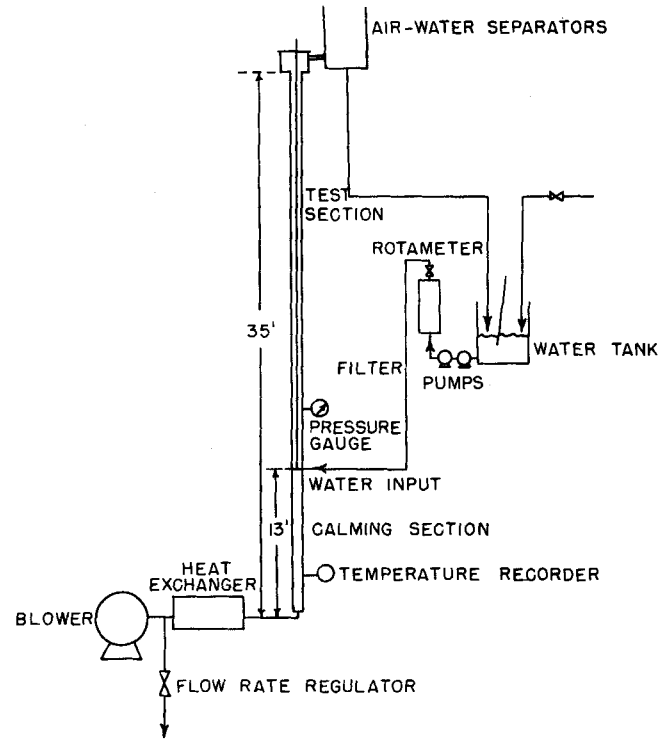

Fig. 2. Schematic flow diagram.

and water injection system. Filtered air was supplied by a blower rated at 550 cu.ft./min. at 9 lb./sq.in. This air was cooled to approximately room temperature before entering the test section. Water was injected through a 1-in. long porous stainless steel section located 2 ft. above the air inlet. This porous section provided circumferentially uniform flow of water, which formed the climbing film on the inner core.

Friction losses were measured by means of static pressure taps. Velocity profiles were determined by means of a Pitot tube made of 0.02-in. O.D. hypodermic needle tubing. The

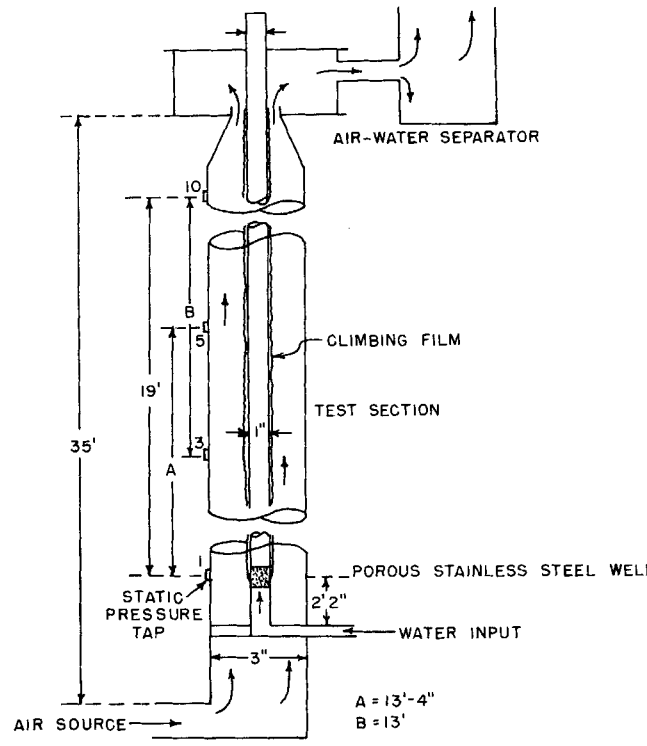

Fig. 3. Test section.

tube was mounted on a traversing mechanism and the position determined with a Tumico dial indicator with a 1-in. range and with 0.0005-in. scale divisions.

A calibrated Preston (*14*) tube made of 0.0544-in. O.D. stainless steel hypodermic needle tubing was used to measure directly the shear stress on the dry outer wall at points 3 and 5.

The mean film thickness of the climbing film and wavelength and amplitude of surface waves were determined photographically. Photographs were obtained through the transparent outer tube with a 1-ft. long magnifier box, a Hasselblad model 1000 F camera, and a model 1531-A General Radio electronic stroboscope. Two lengths of hypodermic needle tubing were placed a short distance from the inner core and in a plane passing through the axis of the annular duct. These served as a reference by which the thickness of the film could be measured. The light from the stroboscope was arranged so that it came from behind the duct and in this way a sharp outline of the air–water interface was visible.

EXPERIMENTAL PROGRAM

The investigation is divided into many parts. These include pressure loss measurements, air velocity profile measurements, direct determination of shear stresses on the outer wall, photographing of the film, and subsequent determination of film thickness and wavelength of surface waves.

Air flow rates varied from 800 to 1,500 lb./hr. Two water flow rates were used: 0.47 and 0.79 lb./min. At water flow rates greater than 0.8 lb./min. breakup of the film occurred at the points where the centering pins were located. Further streamlining of the centering pins is necessary to attain a stable film at higher water flow rates.

RESULTS AND DISCUSSION

Pressure Losses

Pressure losses were determined across taps 3 and 5 and taps 5 and 10 (Figure 3). These are referred to, respectively, as the top and bottom locations. Figure 4 is a plot of experimental pressure gradients as a function of air mass flow rate for the lower region with water flow rate as the parameter.

Friction factors calculated from Equations (1) and (3) with λ defined by Equation (4) are plotted for the same region in Figure 5. The smooth pipe curve represents Equation (3). Single-phase flow friction factors obtained in the present work are 4 to 14% above the Nikuradse equation. Brighton and Jones (*1*) reported annular friction factors approximately 10% higher than those predicted by Nikuradse's equation.

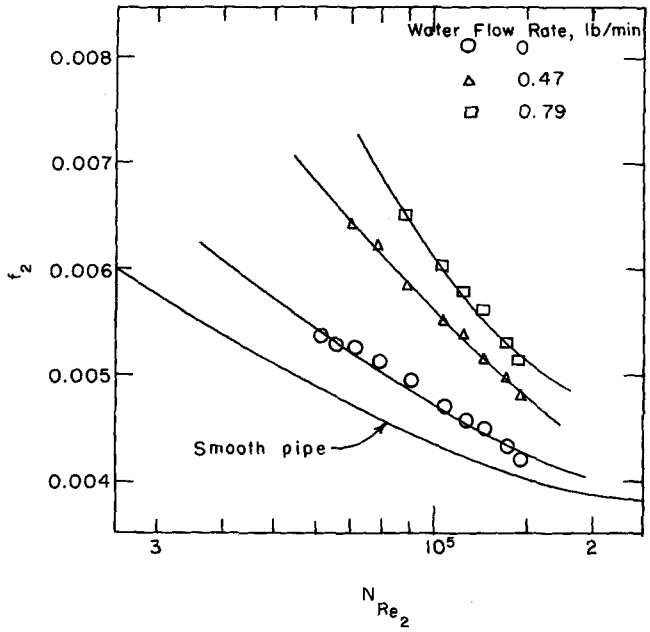

Fig. 5. Friction factors vs. air Reynolds numbers for region between taps 3 and 5.

Pressure gradients in the top region (between taps 5 and 10) were about 7% greater than those in the bottom region. This discrepancy could be due to entrainment, undeveloped flow, variations in roughness of flange connections and variations in concentricity of the inner core, although every attempt was made to eliminate these effects during the construction of the test section. Single-phase flow friction factors obtained were considered in reasonable agreement with results of previous workers.

Pressure losses were correlated in Figure 6 where Φ and X are the Lockhart and Martinelli (*9*) parameters for two-phase flow in tubes.

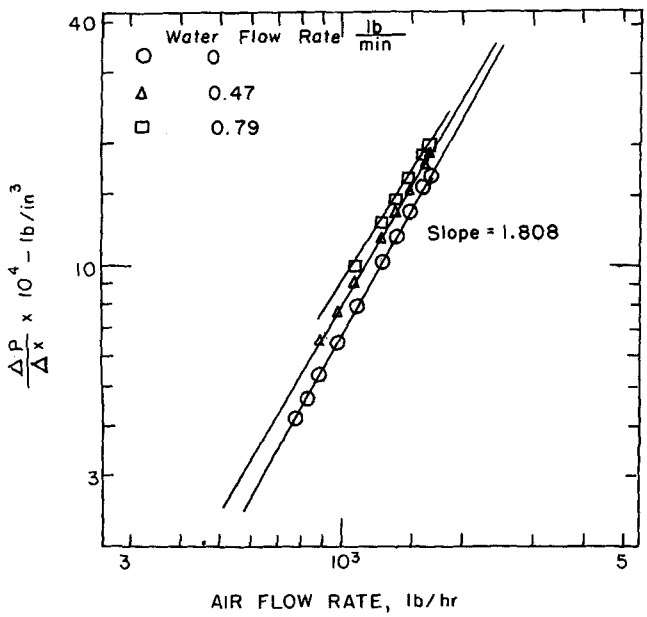

Fig. 4. Pressure losses between taps 3 and 5.

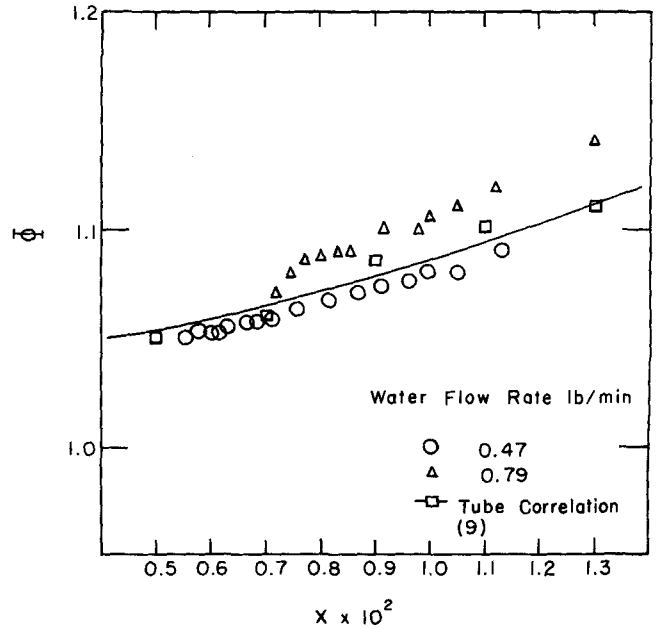

Fig. 6. Pressure loss correlation for annular channel.

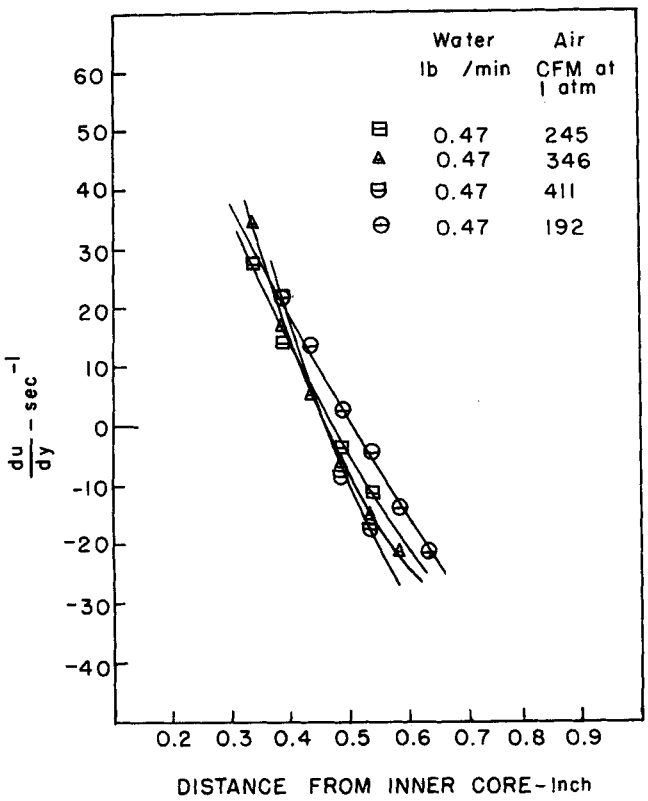

Fig. 7. Velocity gradients near region of maximum velocity at bottom location.

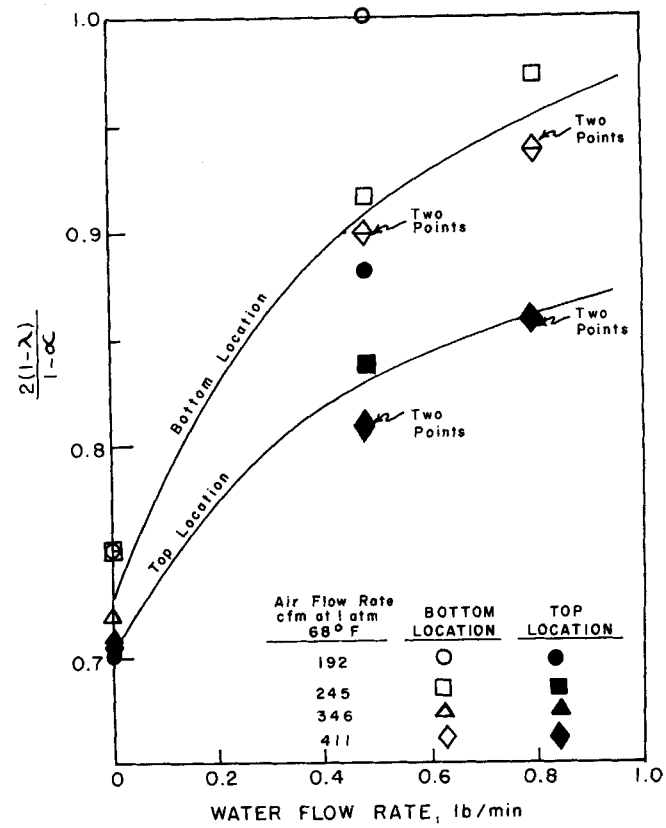

Fig. 9. Position of point of maximum velocity in annular duct as a function of water flow rate.

$$\Phi^2 = \left(\frac{dP}{dx}\right)_{TP} \Big/ \left(\frac{dP}{dx}\right)_g \qquad (28)$$

$$X^2 = \left(\frac{dP}{dx}\right)_L \Big/ \left(\frac{dP}{dx}\right)_g \qquad (29)$$

where $(dP/dx)_{TP}$ is the pressure gradient of climbing film flow (two-phase flow), and $(dP/dx)_L$ and $(dP/dx)_g$ are pressure gradients in the annulus when liquid and gas, respectively, flow alone in the channel. Because the liquid Reynolds number (flowing alone in the annulus) was less than 2,000 ($N_{ReL} < 10$), $(dP/dx)_L$ was calculated from the equation

$$\left(-\frac{dP}{dx}\right)_L = \frac{32\,\mu\,U}{g_c\,(d_2^2 - d_1^2 - 2\,d_m^2)} \qquad (30)$$

The solid curve is the Lockhart–Martinelli correlation in tubes for viscous liquid and turbulent gas flow as expressed in analytical form by Hewitt, King, and Lovegrove (3). The agreement between the present data and the solid line is within 7%. Thus the correlation for two-phase flow in tubes is recommended for the estimation of pressure losses in climbing film flow in an annular duct for the range of air and water flow rates studied. However, it is necessary to study high water flow rates to reach a more general conclusion concerning the correlation.

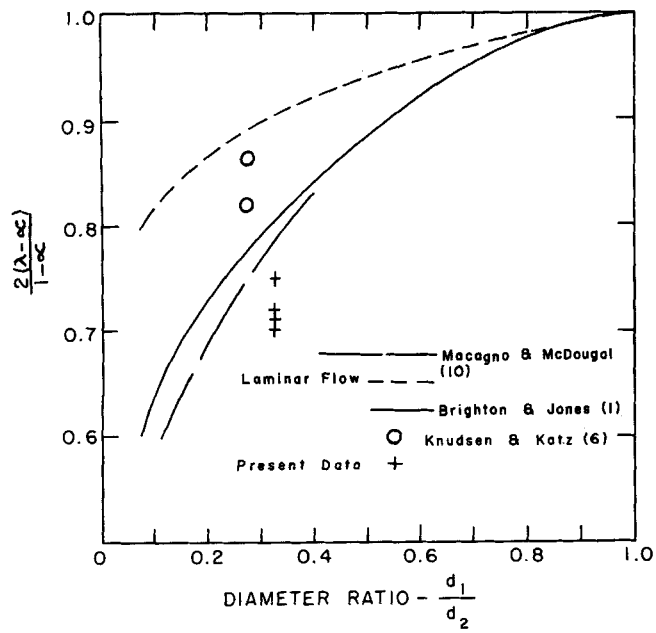

Fig. 8. Points of maximum velocity for single turbulent phase flow in annuli.

Air Velocity Profiles

Air velocity profiles were obtained at both the top and bottom locations (3 and 5 in Figure 3) at several different air flow rates and two water flow rates. The point of maximum velocity was of particular interest in this study. Therefore point velocities were obtained every 0.02 in. throughout the region of maximum velocity. The point of maximum velocity was obtained by a numerical technique in which the velocity gradient du/dr was calculated from five values of the point velocity. By assuming that the velocity profile curve can be fitted to a low degree polynomial, say a quadratic, the velocity gradient at the central point of five equally spaced points is

$$\left.\frac{du}{dy}\right|_{u_0} = \frac{-u_{-2} - u_{-1} + u_1 + u_2}{\Delta y} \qquad (31)$$

Calculated values of du/dy are plotted vs. the distance from the inner wall in Figure 7 for the bottom location

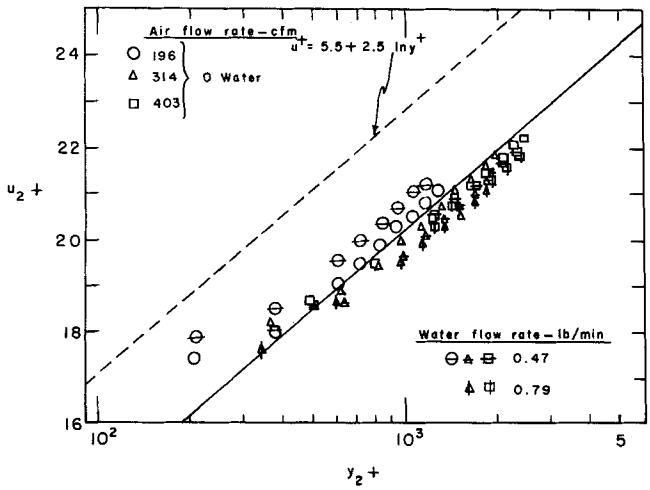

Fig. 10. Velocity distribution for the outer portion of the annular profile.

and a water flow rate of 0.47 lb./min. The point where $du/dy = 0$ is considered the point of maximum velocity.

Points of maximum velocity for single-phase flow are shown in Figure 8 as a function of d_1/d_2. For comparison the curve for laminar flow and the curve for turbulent flow reported by Brighton and Jones and the theoretical curve of Macagno and McDougall are shown. The turbulent flow data reported by Knudsen and Katz (*6*) were also analyzed according to Equation (31) and are plotted in Figure 8. Figure 8 indicated that the position of maximum velocity for turbulent flow is closer to the inner tube than for laminar flow but considerable variation exists among the data. The present data are about 15% below the results of Brighton and Jones. These results may have been caused by certain roughness of the flange connections on the outer tube. The points of maximum velocity for the top location were slightly closer to the inner tube than for the lower location.

The position of the point of maximum velocity as it is affected by the presence of the water film on the inner core is shown in Figure 9. The film has the effect of shifting the point of maximum velocity toward the outer tube. A similar result would be obtained by roughening the surface of the inner core and indicates the presence of higher shear rates at the water surface than are present when the core is dry.

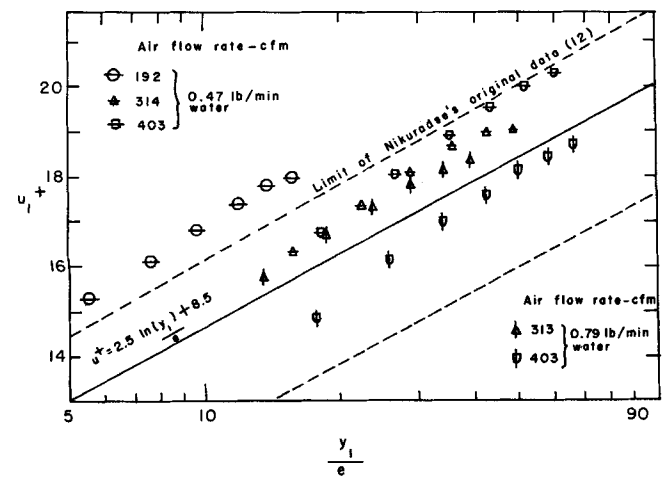

Fig. 11. Velocity distribution for the inner portion of the annular velocity profile.

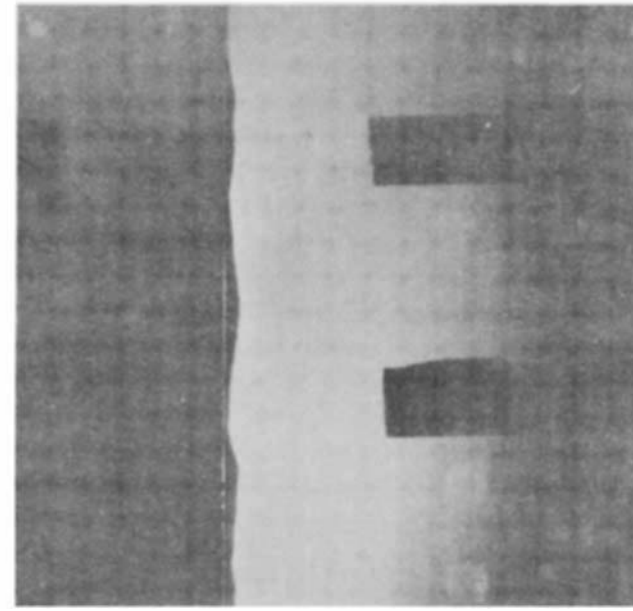

Fig. 12. Photograph of climbing film (air flow = 245 cu.ft./min.; water flow = 0.79 lb./min.).

The air velocity distribution data are correlated in Figures 10 and 11. Figure 10 is a plot of u_2^+ vs. y_2^+ for the outer portion of the annular velocity profile. All data are represented reasonably well by the solid line expressed by the equation

$$u_2^+ = 3.0 + 2.5 \ln y_2^+ \qquad (32)$$

Equation (32) was reported by Knudsen and Katz (*6*) for single-phase flow of water. It appears that the presence of the water film does not affect the outer velocity profile (although the position of maximum velocity is affected) and the same equation may be used to predict point velocities for single-phase flow as for two-phase flow.

An approximate correlation of the inner velocity profile data is shown in Figure 11, where u_1^+ is plotted vs. y_1/e and e is the average height of the waves on the water film. This quantity had a value approximately twice the mean film thickness reported in a subsequent section. This average value was obtained from photographs of the water film taken at the time the velocity profile was determined. The solid line in Figure 11 is represented by

Table 1. Film Characteristics

Air flow rate, cu. ft./min. at 68°F. 1 atm.	Measured water flow rate, lb./min.	Film thickness h_0, in.	Wave amplitude, in.	Wavelength, in. $2\pi/k$ Measured	Wavelength, in. $2\pi/k$ Predicted Equation (24)	Predicted water flow rate, lb./min.
198	0.47	0.0127	0.012	0.20		0.356
245	0.47	0.0049	0.005	0.15		
288	0.47	0.0041	0.004	0.13		
318	0.47	0.0040	0.004	0.09	0.026	0.244
350	0.47	0.0037	0.0035	0.08		
385	0.47	0.0029	0.003	0.06		
402	0.47	0.0026	0.003	0.055	0.018	0.243
245	0.79	0.008	0.008	0.13		
288	0.79	0.0059	0.006	0.10		
318	0.79	0.0043	0.004	0.08	0.024	0.46
350	0.79	0.0043	0.004	0.06		
385	0.79	0.0031	0.003	0.06		
402	0.79	0.0024	0.0024	0.065	0.011	0.32

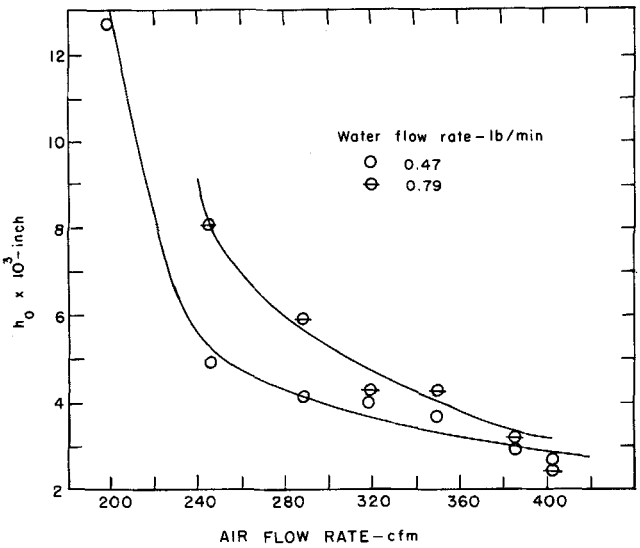

Fig. 13. Film thickness as a function of air flow rate.

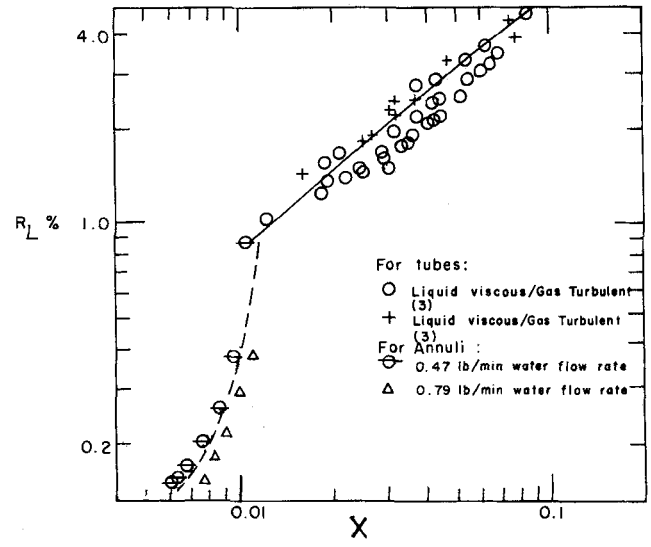

Fig. 14. Film thickness correlation.

$$u_1^+ = 2.5 \ln y_1/e + 8.5 \qquad (33)$$

an identical relation to that proposed by Nikuradse (*11*) for the velocity profile in rough tubes. The broken lines indicate the range of data used by Nikuradse in obtaining his rough tube correlation.

Film Characteristics

A typical photograph of the profile of the water film is shown in Figure 12. Film thickness, amplitude, and wavelength were determined from many such photographs. The results are presented in Table 1. Film thickness was obtained by measuring the distance of the film from a line joining the two reference probes and comparing this to the distance of the inner core from the same line. An analysis of this procedure indicates the possibility of a maximum error of ± 0.002 in which indicates maximum percent error up to 100% for some of the film thicknesses shown. The thicknesses shown in Table 1 are the result of measurements on a large number of photographs and reasonably consistent results are obtained as is shown in Figure 13. The thickness decreases rapidly up to a flow rate of 240 cu.ft./min. after which it decreases more slowly, becoming nearly independent of water flow rate at the highest air flow rate studied.

Mean film thickness is correlated in Figure 14 by the parameter R_L (*9*), which is the fraction of liquid holdup:

$$R_L = \frac{\alpha_i^2 - \alpha^2}{1 - \alpha^2} \qquad (34)$$

The data above $X = 0.01$ were reported by Hewitt et al. (*3*) for climbing film flow in a circular tube. The solid line is the suggested extrapolation by these workers of the original Lockhart–Martinelli correlation for the small X region. The broken line representing the present data is quite different. The present results, however, approach the solid line and it would appear that the region in the vicinity of $X = 0.01$ is a transition region. The main differences between the two sets of data shown in Figure 14 are: (1) The present data were obtained in a circular tube. Lockhart and Martinelli proposed that their correlation was suitable both for annuli and circular tubes. (2) The present data were obtained at minimum rates of entrainment. Hewitt et al. obtained holdup data under high entrainment conditions. The present investigation was continued only up to the point where entrainment occurred. This could explain the apparent existence of a transition point at $X = 0.01$, the broken line representing holdup under conditions of no entrainment and the solid line representing holdup under conditions of entrainment.

The wave shapes shown in the photographs were quite irregular. Wavelength was determined in each photograph by dividing the number of peaks by the length of liquid film shown in the photograph. Wavelength decreases with increasing air flow rate indicating a greater rate of energy transfer from the air to the film.

The amplitude of the waves was approximately equal to the mean film thickness. The ratio of wavelength to amplitude varied from 20 to 30. On the basis of a criterion proposed by Brooke-Benjamin (*2*) laminar wave motion existed in all climbing films studied.

The theoretically derived Equations (23) and (24) may be used to predict the mean film thickness and wavelength. It is more convenient to combine Equation (23) with Equations (9) and (10) to obtain

$$\frac{3\nu Q}{2\pi r_1 g_c} = \left[\frac{r_2 - \lambda^2 r_2^2}{2r_2}\left(\frac{-dP}{dx}\right)\right.$$
$$\left.\frac{\lambda^2 r_2^2 - (r_1 + h_0)^2}{r_2^2 - \lambda^2 r_2^2}\,\frac{r_2}{r_1}\right]\frac{3h_0^2}{2\rho_L} - \left(\frac{1}{\rho_L}\frac{dP}{dx} + \frac{g}{g_c}\right)h_0^3 \qquad (35)$$

Equation (35) may be used to calculate Q from h_0. Predicted values of water flow rate and wavelength appear in Table 1. Predicted flow rates are about one half of measured flow rates. Since in Equation (35) the flow rate is dependent on h_0^2 and h_0^3, a small error in the measured value of h_0 could cause a large error in the predicted value of the flow rate. Predicted values of wavelength are one fourth to one fifth of the measured values. The development based upon Kapitza's theory of wave formation therefore predicts film thicknesses in reasonable agreement with measured values but apparently is not reliable in predicting wavelength of capillary waves formed on the climbing film surface. Further study is required.

Shear Stresses

When the film thickness, position of maximum velocity, and pressure loss are known, Equations (8), (9), and (10) may be used to calculate shear stresses. In addition, the shear stress at the outer wall of the annulus was measured directly by means of a calibrated Preston tube. The various shear stresses for several flow rates appear in

TABLE 2. SHEAR STRESSES AT TOP LOCATION

Air flow rate, cu. ft./min. at 68°F. 1 atm.	Water flow rate, lb./min.	Shear stresses, lb./sq. ft. × 10^4: τ_2 measured by Preston tube	τ_2 calculated from Equation (9)	τ_i calculated from Equation (10)	τ_1 calculated from Equation (8)
196	0	2.90	2.95	——	2.74
	0.47	2.95	2.96	3.94	−0.41
245	0	4.26	4.48	——	4.16
	0.47	4.42	4.63	5.79	3.87
314	0	6.52	6.58	——	6.09
	0.47	6.70	6.92	8.14	6.79
	0.79	6.90	7.16	9.37	7.61
403	0	9.35	9.32	——	8.65
	0.47	9.70	9.68	11.42	10.34
	0.79	9.90	9.93	13.08	11.97

Table 2. Good agreement is obtained between τ_2 measured by the Preston tube and τ_2 calculated from Equation (9).

In general, τ_2 is nearly independent of water flow rate, a result which could be expected from the velocity profile correlation shown in Figure 10 for the outer portion of the velocity profile.

Higher shear stresses exist at the air–water interface (τ_i) than at the water–solid interface τ_1. At the lowest air flow rate the shear stress τ_1 assumes a negative value. This suggests that some downflow occurs in the film adjacent to the wall. However, the net flow is upward and the velocity profile in the film could be of the shape shown in Figure 15*a*. At higher flow rates this downflow would not occur and a velocity profile similar to that shown in Figure 15*b* would exist.

CONCLUSIONS

The characteristics of climbing film flow for air and water flowing in an annular duct have been investigated with respect to pressure losses, film characteristics, and air velocity profiles. The following conclusions and results are obtained:

1. Friction factors for single-phase air flow in the annular duct are 4 to 14% above those predicted by the Nikuradse equation when the equivalent diameter of the outer portion of the annular velocity profile is used as the characteristic length term. Friction factor results agree well with those of Brighton and Jones.

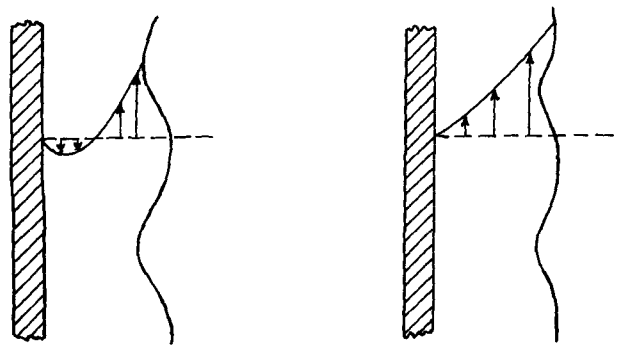

(a) Low Air Flow Rate (b) High Air Flow Rate

Fig. 15. Possible velocity profiles in liquid film.

2. Pressure losses for two-phase climbing film flow in the annular duct may be correlated with the Lockhart–Martinelli parameters and the correlation agrees with that proposed by these workers for laminar liquid–turbulent gas flow in tubes.

3. The position of maximum velocity of the annular air stream moves toward the outer wall with increasing liquid flow rate. This suggests that the climbing film creates a rough wall condition.

4. The shear stress on the outer dry wall is nearly independent of water flow rate while the outer velocity distribution is given by the relation

$$u_2^+ = 3.0 + 2.5 \ln y_2^+ \qquad (32)$$

5. The velocity distribution for the inner portion of the velocity profile is correlated by the Nikuradse equation

$$u_1^+ = 8.5 + 2.5 \ln y_1/e \qquad (33)$$

indicating that the film creates a rough wall condition.

6. Film thickness (holdup) may be correlated by Lockhart–Martinelli parameters. There are indications that the present data obtained under conditions of no entrainment follow one holdup correlation, while data obtained under entrainment conditions follow a different correlation.

7. Application of Kapitza's theory of wave formation to the calculation of film thickness and wavelength was only partially successful. The theory predicts reasonable values of film thickness but gives wavelengths which are 1/4 to 1/5 of the measured value.

8. An investigation of the shear stresses at the various interfaces in the annular duct suggests that at low air flow rates there is downflow in part of the climbing film. Data are too meager to reach definite conclusions concerning this phenomenon.

ACKNOWLEDGMENT

The authors wish to express their appreciation to the National Science Foundation for a research grant GP-502 under which this study was performed.

NOTATION

c = wave celerity, L/t
d_1 = inner core outside diameter
d_2 = outer tube inside diameter, L
F = force
f_2 = friction factor as defined by Equation (2)
g = acceleration of gravity, L/t^2
g_c = force-mass conversion factor, mL/sq.ft.
h = instantaneous film thickness
h_0 = mean film thickness, L
k = wave number (wavelength is $2\pi/k$)
L = length
m = mass
N_{Re_2} = Reynolds number as defined by Equation (1)
P = static pressure
ΔP_f = pressure difference due to friction
P_σ = surface pressure
P_g = gas stream pressure, F/L^2
Q = water flow rate, L^3/t
q = heat flux, F/tL
r = radius
r_1 = inner core radius
r_2 = outer tube radius
r_i = interface radius
r_H = equivalent diameter of outer portion of annular velocity profile
r_m = radius of point of maximum velocity, L
R_L = $r_1^2 - r_1^2/r_2^2 - r_1^2$
t = time

U = mean velocity, L/t
u, v = point velocity
u^* = friction velocity, $\sqrt{\tau_w/\rho}$
u^+ = u/u^*
u_0 = velocity at average stream cross section h_0
$\bar{u}$ = average velocity of film of thickness h
X = parameter as defined by Equation (29)
x, y = direction coordinate, L
y^+ = dimensionless distance, $yu^*\rho/\mu$
y_1 = distance from the inner wall
y_2 = distance from the outer wall, L

Greek Letters

α = r_1/r_2, α_1 r_i/r_2
μ = coefficient of viscosity, m/Lt
ν = kinematic viscosity, L^2/t
ρ = density
ρ_g = density of air
ρ_L = density of water, m/L^3
σ = coefficient of surface tension of water, F/L
τ = shear stress
τ_1 = shear stress on the inner wall
τ_2 = shear stress on the outer wall
τ_i = shear stress at air–water interface, F/L^2
ϕ = function as defined by Equations (26) and (27)
Φ = parameter as defined by Equation (28)
λ = r_m/r_2

LITERATURE CITED

1. Brighton, J. A., and J. B. Jones, *J. Basic Eng.*, **86**, 835 (1964).
2. Brooke-Benjamin, T., *J. Fluid Mech.*, **2**, 554 (1957).
3. Hewitt, G. F., R. D. King, and P. C. Lovegrove, *AERE-R3921*, U.K. Atomic Energy Authority, Harwell, Berks. (1962).
4. Kapitza, P. L., *J. Exptl. Theoret. Phys.* (Russian), **18**, 3 (1948).
5. Kim, D. H., Ph.D. *thesis*, Oregon State Univ., Corvallis (June, 1965).
6. Knudsen, J. G., and D. L. Katz, *Proc. First Midwest Conf. Fluid Dynamics*, Univ. Illinois, 175 (May, 1950).
7. ———, "Fluid Dynamics and Heat Transfer," McGraw-Hill, New York (1958).
8. Levich, V. G., "Physicochemical Hydrodynamics," Prentice-Hall, Englewood Cliffs, N. J. (1962).
9. Lockhart, R. W., and R. C. Martinelli, *Chem. Eng. Progr.*, **45**, 39 (1949).
10. Macagno, E. O., and D. W. McDougall, *A.I.Ch.E. J.*, **12**, 437 (1966).
11. Nikuradse, J., *VDI Forschungsh.*, 356 (1932).
12. *Ibid.*, 361 (1933).
13. Prengle, R. S., and R. R. Rothfus, *Ind. Eng. Chem.*, **47**, 379 (1955).
14. Preston, J. H., *J. Roy. Aeronaut. Soc.*, **58**, 109 (1954).

Manuscript received January 13, 1966; revision received August 15, 1966; paper accepted August 15, 1966.

A Method for the Noninteracting Control of a Class of Linear Multivariable Systems

ROBERT D. FOSTER

Union Carbide Chemicals Company, South Charleston, West Virginia

WILLIAM F. STEVENS

Northwestern University, Evanston, Illinois

A method is presented by which a particular class of interacting linear multivariable systems may be decoupled into independent, first-order subsystems containing a single output as a function of a single manipulatable input and a single measurable input. This is accomplished by application of compensators in the form of feedforward amplifiers and proportional plus derivative feedback controllers. Simultaneous application of a stabilizing feedback controller and a feedforward amplifier to each decoupled subsystem results in perfect control of system outputs $y_i(t)$, that is, $y_i(t) = 0$ for all $t \geqq 0$. In addition, the compensating device contains degrees of freedom that make it possible to set output forms within any limits desired in the case that subsystem feedforward controllers operate imperfectly, and obtain better fit between the linear system model, which forms the basis for controller design, and the corresponding nonlinear system model.

A physical system is defined as multivariable when it has a multiplicity of inputs and outputs. The most important characteristic of such systems is that they will generally be interacting or cross coupled, a condition that occurs when there are inputs which simultaneously affect more than one output. Kavanagh (*4, 5*) was the first to apply rigorously matrix methods to the analysis of such systems and his work is a framework for a basic understanding of the properties of multivariable control systems.

If conventional control is applied to any output y_i of a multivariable system, it will not generally be possible to eliminate the effect of other controller signals or external upsets on y_i. These cross effects may, in addition, be of sufficient magnitude to make it impossible to control y_i